Dalton Transactions

Accepted Manuscript

ROYAL SOCIETY OF CHEMISTRY

www.rsc.org/dalton

Dalton Transactions

ARTICLE

The synergy between Ti species and g-C_3N_4 by doping and hybridization for the enhancement of photocatalytic H_2 evolution

Received 00th January 20xx,
Accepted 00th January 20xx

DOI: 10.1039/x0xx00000x

www.rsc.org/

Xiao-jing Wang, Xiao Tian, Fa-tang Li*, Jun Zhao, Yu-pei Li, Rui-hong Liu, and Ying-juan Hao

A Ti species modified g-C_3N_4 photocatalyst was synthesized via an in-situ hydrothermal route and the following low-temperature calcination. The hydrothermal process results in not only the fabrication of TiO_2/g-C_3N_4 heterojunctions, but also the coordination between Ti species and g-C_3N_4, which are verified by X-ray diffraction (XRD), and X-ray photoelectron spectroscopy (XPS). The electrical resistance test confirms that the coordination can improve the electrical conductivity of composite and make the charge transfer easier. The photoluminescence (PL) and photocurrent measurements exhibit that the hybridization enhances the separation efficiency of photo-induced electrons and holes. As a result, the Ti species modified g-C_3N_4 photocatalysts exhibit much higher photocatalytic H_2 evolution than the simplex heterojunction of TiO_2/g-C_3N_4 obtained via microwave method and the mechanical mixture of TiO_2 and g-C_3N_4 under visible-light irradiation. The coordination mechanism and synthesis route of TiO_2/g-C_3N_4 heterojunctions are proposed.

1. Introduction

Because of the global warming and energy crisis, more attention has been focused on the production of clean energy. Hydrogen is considered to be an attractive fuel due to its high conversion efficiency and zero carbon emission. In the past three decades, photocatalytic water splitting to produce hydrogen has attracted extensive concerns. Notably, as a typical semiconductor photocatalyst, TiO_2 photocatalyst is still a major aspect since its low cost and high chemical stability. Unfortunately, due to its large band gap, TiO_2 can only respond to ultraviolet (UV) light that accounts for about 4% of solar energy, which limits its practical applications.[1,2]

In 2009, a metal free polymeric semiconductor, graphite-like carbon nitride (g-C_3N_4), was reported by Wang et al.[3] Owning to its non-toxicity, chemical and thermal stability, and good photocatalytic hydrogen production ability, g-C_3N_4 has received increasing attention both in the fields of photocatalysis and photoelectrochemistry. In addition, the composition of g-C_3N_4 is earth-abundant, and it can be easily fabricated and thus is commercially available. However, the rapid recombination rate of photo-generated electron-hole pairs of pure g-C_3N_4 leads to its low quantum efficiency. Various modifications have been employed to improve the photocatalytic activity of g-C_3N_4, such as structural adjustment,[4-6] surface modification,[7-9] element doping,[10-13] and coupling with other semiconductor materials.[14-20] From the point of view of the enhancement of electrical conductivity, chemical doping is an effective strategy.[10,21,22] Coupling with other semiconductors (such as BiOX,[15] CdS,[16] Al_2O_3,[17,18] TiO_2,[19,20] etc.) is an effective way for lowering the recombination rate. It is worth noting that the band edge position of TiO_2 is matched well with that g-C_3N_4 during the process of photocatalytic water splitting to produce hydrogen.[19] Thus, many studies have been reported on the fabrication and photocatalytic applications of TiO_2/g-C_3N_4 composites.[19,20,23-31] We also synthesized the TiO_2/g-C_3N_4 heterojunction via microwave assistance, in which the highly dispersed interface between TiO_2 and g-C_3N_4 facilitated the migration of photo-generated electrons.[31] Nevertheless, most of the synthetic methods of TiO_2/g-C_3N_4 composites need organic solvents, titanium alkoxides and high temperature. Moreover, the physical properties of g-C_3N_4 in the composites are unchanged for the most part. To the best of our knowledge there are no reports till date on lowering the recombination rate of photo-generated electrons by coupling and simultaneous improving electric conductivity by doping.

In the present work, a facile and effective method is presented to fabricate Ti species modified g-C_3N_4 with the enhancement of photocatalytic performance. This in-situ hydrothermal synthetic route results in coordination between Ti species and g-C_3N_4, which improves the electronic conductivity of the composite, and the hybridization of TiO_2 and g-C_3N_4 facilitates the separation of charge carriers. The photocatalytic performances are systematically evaluated by photocatalytic hydrogen production under both visible-light and simulated sunlight. According to the results of the experiments, the photocatalytic mechanism of Ti species modified g-C_3N_4 is proposed. This work could provide deeper insight into the enhanced mechanisms of π-conjugated molecules hybridized semiconductors.

College of Science, Hebei University of Science and Technology, Shijiazhuang 050018, China.Email: lifatang@126.com.

2. Experimental

2.1 Preparation of catalysts

All starting materials were purchased from commercial sources and were used without further purification. The bulk g-C_3N_4 was synthesized by thermal polycondensation of melamine according to previous paper.[3] Typically, melamine in a covered crucible was calcined in a muffle furnace with a heating rate of 10 °C/min to 550 °C where it was held for 3 h. The product was collected and ground into powder for further usage and performance measurements.

Metatitanic acid was selected as the Ti reactants. Firstly, 20 mL of H_2O_2 (30 wt%), 5 mL of $NH_3 \cdot H_2O$ (28 wt%), and 10 mL deionized water were mixed in an ice-cooled bath to obtain mixture. Then the mixture was divided into two parts equally. Secondly, a designed amount of metatitanic acid was added into on part mixture. After stirring for 30 min, a homogeneous peroxotitanate solution was obtained. Thirdly, 0.5g of the prepared g-C_3N_4 was dispersed into the other part mixture and treated by an ultrasonic disperse method for 30min. Subsequently, the peroxotitanate solution was mixed with the g-C_3N_4 suspension. After stirring for 4h, the mixture was transferred into a 50 mL Teflon reactor inside a stainless-steel vessel and heated at 160 °C for 4 h. After reaction, the products were separated by filtration, thoroughly washed with deionized water and then dried at 80 °C. Finally, The obtained samples were calcinated at 180-500 °C in a muffle furnace for 2 h. The obtained samples were named as XTC-Y, where X and Y are the theoretical percentage mass content of TiO_2 based on the precursor ratio and calcination temperature of the samples, respectively. Pure TiO_2 and 0TC-300 were prepared under the same conditions in the absence of g-C_3N_4 or metatitanic acid. For comparison, TiO_2/g-C_3N_4 composite (25.4 wt% TiO_2) was also synthesized by a microwave-assisted route,[31] and named as 20TC-300W. The mechanical mixture of TiO_2 and g-C_3N_4 (26 wt% TiO_2) was named as TC-300M.

2.2 Characterizations

The thermogravimetry (TG)–differential scanning calorimetry (DSC) were performed using a Shimadzu TGA-60H thermal analyzer. The matter phases of as-prepared samples were analyzed by X-ray diffraction (XRD, Rigaku D/MAX 2500 X-ray diffractometer with CuK α radiation). High Resolution transmission electron microscopy (HRTEM) images were taken from a JEOL JEM-2010 electron microscope. Scanning electron microscopy (SEM) was recorded by HITACHI S-4800. The Brunauer-Emmett-Teller (BET) surface area measurements were performed by Micromeritics Tristar II 3020 apparatus. Hitachi F-4600 fluorescence spectrophotometer was used to obtain the photoluminescence (PL) measurements. The X-ray photoelectron spectroscopy (XPS) analysis was carried out on a PHI 1600 ESCA XPS system. All the binding energies were referenced to the C 1s peak at 284.8 eV.

2.3 Electrochemical measurements

Electrochemical measurements were performed by CHI-660E electrochemical workstation. The photocurrent investigation was performed by the three-electrode cell with a working

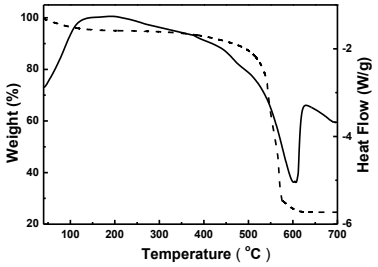

Fig. 1. TG-DSC thermograms for heating the 20TC-300 composite.

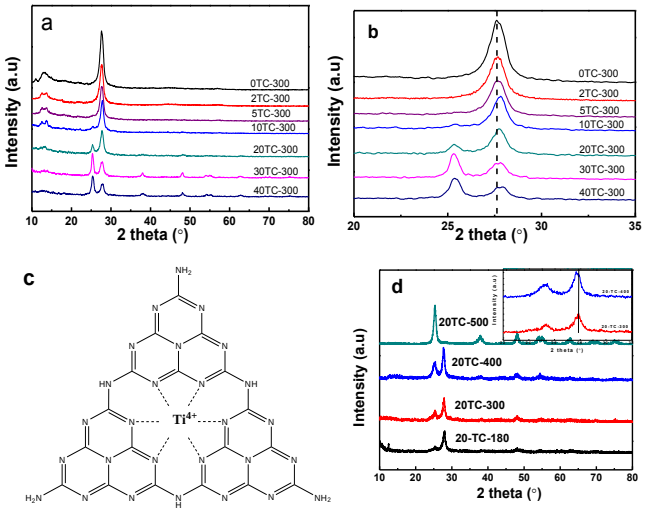

Fig. 2. (a) XRD patterns of g-C_3N_4 and TiO_2/g-C_3N_4 composite calcined at 300°C, (b) magnified XRD patterns of above composites, (c) graphic representation for the coordination between g-C_3N_4 and Ti species, and (d) XRD patterns of 20TC composites calcined at different temperature.

electrode, a platinum electrode as counter electrode, and a saturated calomel electrode as reference electrode. A mixture of aqueous solution with 0.2 M Na_2SO_4 was employed as the electrolyte. The working electrode was prepared as follows: 50mg of the as prepared photocatalyst was dispersed in 1 mL dimethylformamide to produce slurry and then 20 μL of the slurry was spread on cleaned 1.5 cm $\times$ 1.0 cm fluoride-tin oxide (FTO) glass electrode. Finally, the electrodes were calcined at 200 °C for 3 h.

Conductivity measurements were done by confining the sample between two copper discs and measuring the electrical resistance of the respective sample via two probe method.[22,32] 0.2g of the sample was pressed into wafer by a tablet machine under the same constraint. The tablet of the sample was clamped on a copper sample holder assembly between two copper leads. All experiments were performed within a frequency range from 100Hz to 100 kHz and with oscillation amplitude of 50 mV.

2.4 Photocatalytic activity tests

A gas-closed circulation system (Perfect Light Labsolar-III) was used to detect the photocatalytic hydrogen evolution. Xe lamp (300 W, PerfectLight, with 400 nm cut-off filter) was used as the visible-light source. Typically, 100mg photocatalyst powders were dispersed in 100 mL mixed solution containing 5 ml aqueous solution of $H_2PtCl_6 \cdot 6H_2O$, 25 ml triethanolamine (TEOA) and 70 ml deionized water. In this system, TEOA is

acting as a sacrificial reagent to capture the photo-induced holes. Pt (1 wt%) was photo-deposited on the surface of photocatalysts via an in situ route from the precursor of $H_2PtCl_6 \cdot 6H_2O$. In the photocatalytic process, the temperature of the photocatalytic reactions was kept at 15 ° C by condensate pump. The evolved hydrogen was analyzed by thermal conductivity detector (TCD) gas chromatograph (Techcomp GC7900, Ar as a carrier gas) every 1h.

3. Results and discussion

3.1 Characterization of the samples

To investigate the thermal stability and the actual contents of the photocatalysts, TG experiments were carried out. Fig. 1 shows the progress of 20TC-300 heated from room temperature to 700 °C in air. As can be observed, the first mass-loss step was assigned to the absorbed water and the second step with an endothermal peak from 500 °C was assigned to the decomposition of g-C_3N_4 in the composite. The initial decomposition temperature of g-C_3N_4 is lower than that its preparation one, which should be related to the calcination conditions, such as, no cover for the sample 20TC-300 in the TG measurement. Base on the TG experiments, the actual contents of TiO_2 in the composites were calculated, and the results are shown in Table 1. The actual contents of TiO_2 are slightly higher than the precursor ratio, which is due to the decomposition of g-C_3N_4 during the process of synthesis.

Fig. 2a shows the XRD patterns of the prepared g-C_3N_4 and TiO_2/g-C_3N_4 composite calcined at 300° C. It can be seen from Fig. 2a that the bulk g-C_3N_4 (0TC-300) has distinct diffraction peak located at 27.4° and an obscure peak at 13.1° , which are indexed as (002) and (100) planes of g-C_3N_4, respectively (JCPDS NO. 87-1526). For TiO_2/g-C_3N_4 composites, the XRD patterns reveal the coexistence of anatase TiO_2 and g-C_3N_4 when X becomes greater than 10. There is no diffraction peak observed with a lower TiO_2 content. Comparing to bulk g-C_3N_4, the diffraction pattern intensity of the (002) peak in all the composites are apparently decreased. In addition, it can be seen that when the TiO_2 content is higher than 10%, the (002) peak position for TiO_2/g-C_3N_4 composites shift to a slightly higher angle than that of bulk g-C_3N_4 (as shown in Fig. 2b). The (002) peak of g-C_3N_4 is considered to be the characteristic interlayer stacking reflection of conjugated aromatic systems. The weakening and shift of this peak, indicating host-guest interactions and an inhibition of polymeric condensation. Our group[17] have reported that the unoccupied 3p or 3d orbitals of Al ion can coordinate with the lone-pair electrons on N atom in g-C_3N_4, which results in shift of the diffraction peak position of g-C_3N_4. Tonda et al.[33] found that the interactions between Fe species and g-C_3N_4 would cause a shift of the (002) peak in g-C_3N_4. Thus, we speculate the shift is due to that Ti species have dropped into the bulk phase of g-C_3N_4 by coordination at higher concentration of peroxotitanate solution, as shown in Fig.2c. Fig.2d exhibits the XRD patterns of 20TC composite calcined at different temperature. The diffraction peak at 25.4° is attributable to the (101) peak of anatase TiO_2. As calcination temperature increasing, the diffraction peak of TiO_2 becomes narrower and higher, implying that TiO_2 crystals trend to be perfect and grow up into larger particle. No g-C_3N_4 peak is found in the sample when the calcination temperature rises to 500 °C, which indicates the oxidization of g-C_3N_4 in air condition at this temperature.[31] It is worth noting that the diffraction pattern of g-C_3N_4 ((002) peak) in the composite shifts to lower angle and returns to the original position of bulk g-C_3N_4 at the calcinations temperature of 400 °C (inset), which indicated the coordination between Ti species and g-C_3N_4 may be destroyed on this temperature.

Table.1. The actual content of TiO_2 in the composites

Sample	Designed TiO_2 content	Actual TiO_2 content
0TC-300	0%	0%
2TC-300	2%	4.57%
5TC-300	5%	8.26%
10TC-300	10%	15.3%
20TC-300	20%	26.2%
30TC-300	30%	34.6%
40TC-300	40%	43.2%
20TC-300W	20%	25.4%

Fig. 3 presents SEM and TEM images of bare TiO_2, g-C_3N_4 (0TC-300) and 20TC-300. As shown in Fig. 3a and b, bare TiO_2 shows an irregular spheroidal structure with a diameter of 20-50nm and the pure g-C_3N_4 displays aggregated morphologies with smooth flakiness. For the 20TC-300, the existences of TiO_2 particles alter surface roughness of g-C_3N_4, as shown in Fig. 3c. It indicates that TiO_2 particles are deposited on the surface of g-C_3N_4, and the composite structures are formed. In addition, the particle size of TiO_2 seems to be decreased with the adding of g-C_3N_4, suggesting that g-C_3N_4 could suppress the growth of

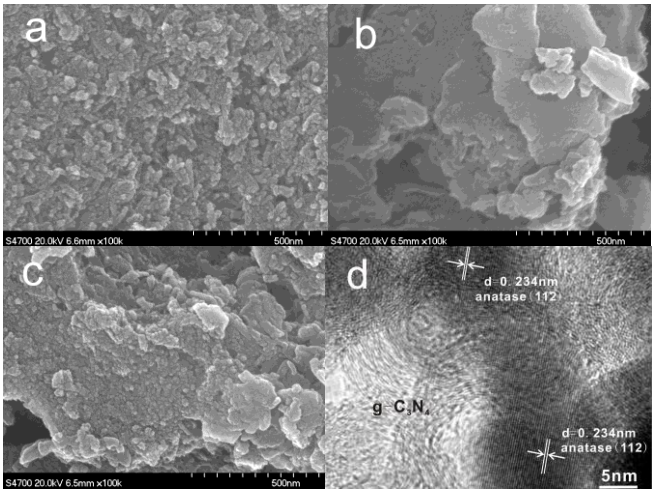

Fig. 3. SEM images of (a) pure TiO_2, (b) g-C_3N_4 (0TC-300), (c) 20TC-300, and (d) HRTEM images of 20TC-300 sample.

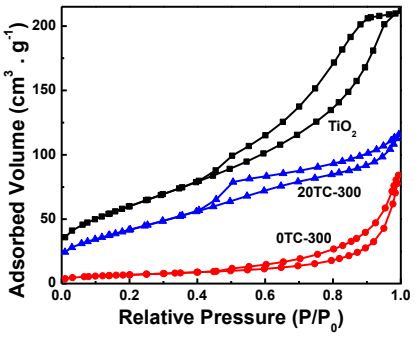

Fig. 4. N_2 adsorption/desorption isotherms of TiO_2, g-C_3N_4(0TC-300) and 20TC-300.

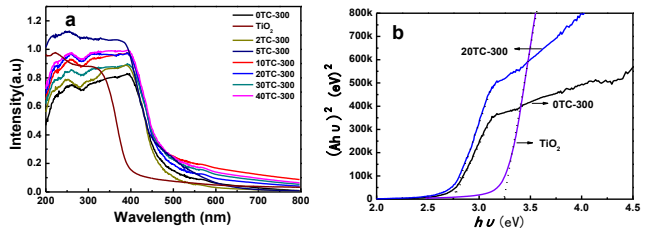

Fig. 5. UV–Vis DRS spectra for as-prepared TiO_2, g-C_3N_4 (0TC-300), and TiO_2/g-C_3N_4 composites.

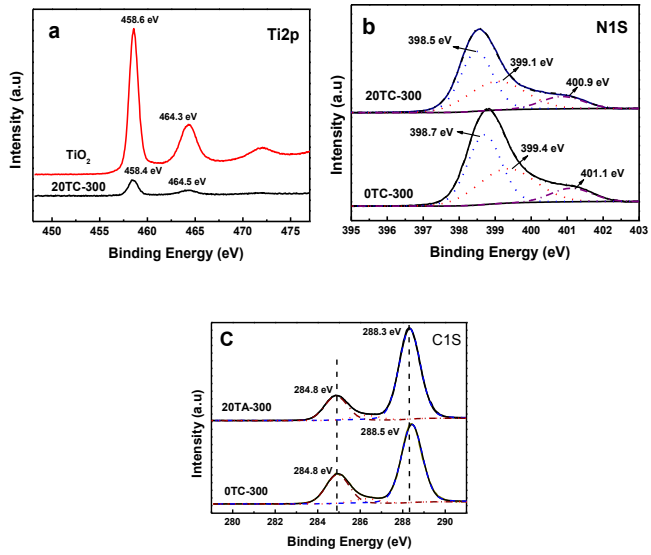

Fig. 6. High resolution XPS spectra of (a) Ti2p, (b) N1s and (c) C1s

TiO_2 particles. Fig. 3d is the TEM image of 20TC-300. The lattice fringe of 0.234 nm is corresponding to the (112) planes of anatase TiO_2. The lattice fringes are clearly observed in TiO_2/g-C_3N_4 composite and the interfaces between the TiO_2 and g-C_3N_4 are smooth, which further proves the existence of heterojunction between TiO_2 and g-C_3N_4.

Fig. 4 indicates the N_2 adsorption-desorption isotherms of various samples of TiO_2, g-C_3N_4 (0TC-300) and 20TC-300. It can be seen that after the hydrothermal treatment, g-C_3N_4 exhibits a type-II nitrogen isotherm with type H3 hysteresis loop, which is believed to be produced by the lamellar stacking of g-C_3N_4 flakes. Pristine TiO_2 and 20TC-300 have typical type IV nitrogen isotherms with H3 hysteresis, which indicating of mesoporous structure. The BET surface areas of the TiO_2, 0TC-300 and 20TC-300 are 218.6, 24.6 and 153.2 m^2/g, respectively. The high BET surface area and mesoporous structure of TiO_2 and 20TC-300 are most likely derived from the decomposition of peroxotitanate, and the release of NH_3 and O_2 during the reaction. The physical characteristics are also beneficial to the adsorption and diffusion of reactant.

The optical absorption properties of TiO_2, g-C_3N_4 (0TC-300) and X-TC-300 are investigated in Fig.5. The main absorption edges of the composites are similar to pure g-C_3N_4.

TiO_2 and g-C_3N_4 are direct transition semiconductor, the band gap energies (Eg) of them can be calculated by a plot of $(\alpha h\upsilon)^2$ versus the photon energy ($h\upsilon$). As shown in the following equation:[34]

$$(\alpha h\nu)^2 = A(h\nu - Eg) \quad (1)$$

where α, h, ν and A are the absorption coefficient, Planck's constant, the light frequency and a constant, respectively. According to Eq. (1), the Eg of the samples can be estimated from a plot of $(\alpha h\upsilon)^2$ versus energy ($h\upsilon$). The interception of the tangent to the X axis would give a good approximation of the Eg of the samples. Thus, the band gaps of TiO_2, g-C_3N_4 and X-TC-300 could be estimated. As seen form Fig. 5b, the Eg of pure TiO_2 and g-C_3N_4 are 3.25 and 2.75 eV, respectively. The composites exhibited a similar absorption property with g-C_3N_4, where the Eg of the composites are absolutely similar to bare g-C_3N_4. This result indicates that the introduction of Ti species has no obvious effect on the optical absorption properties of g-C_3N_4.

In order to further detect the interaction between Ti species and g-C_3N_4, XPS analysis was employed to study the chemical status of the Ti, N, C and O elements in the TiO_2, g-C_3N_4, and TiO_2/g-C_3N_4 composites. Fig. 6a shows the XPS spectrum of Ti2p in bare TiO_2 and 20TC-300. As indicated in Fig. 6a, the binding energies at 458.6 and 468.3 are assigned to Ti2p3/2 and Ti2p1/2. The shift of binding energies value of 20TC-300 can demonstrate the interaction between Ti species and g-C_3N_4 in the composites. The interaction between Ti species and g-C_3N_4 can change the electronic structure of Ti element in the catalyst which affects the effective positive charge on the Ti element.[35] Fig. 6b shows the high-resolution spectra of N1s. After Gaussian curve fitting, the N1s curve could be deconvolved into three peaks at 398.7, 399.4, and 401.1 eV. The two peaks at 399.4 and 401.1 eV can be assigned to tertiary nitrogen (N-C3) and amino functional groups having a hydrogen atom (C-N-H) .The peak at 398.7 eV is typically attributed to N atoms sp2 -bonded to two carbon atoms (C=N-C).[30,36] After introducing Ti species, the binding energy of the three peaks is drifted slightly, verifying the interaction between Ti species and g-C_3N_4. A similar phenomenon is also obtained in the high-resolution spectra of C 1s. The peak at around 284.6 eV is assigned to carbon atoms from contaminated carbon, whereas the peak at 288.5 eV

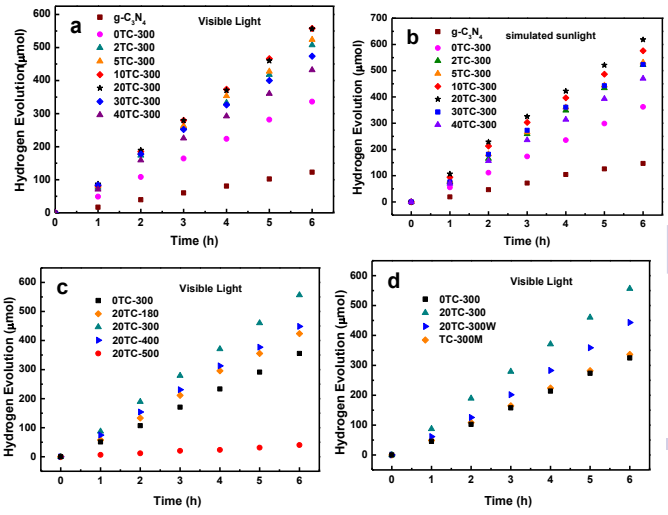

Fig. 7. Photocatalytic H_2 production performance of the samples

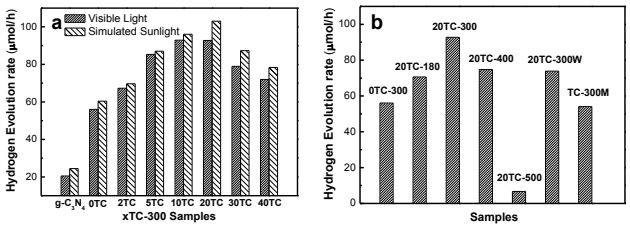

Fig. 8. Average H_2 evolution rate in 6 h over the photocatalysts.

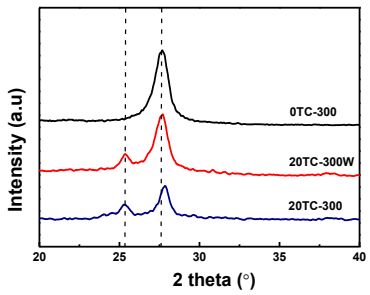

Fig. 9. XRD patterns of 0TC-300, 20TC-300W, and 20TC-300.

identified as originating from carbon atoms bonded to three nitrogen atoms.[37] A feeble shift of the C1s in 20TC-300 also shows the effect of Ti species on g-C_3N_4. All above results can support the conclusion that there is chemical interaction existed between the Ti and g-C_3N_4.

3.2 Photocatalytic H_2 production performance

Fig. 7 shows the photocatalytic activities for hydrogen production of the samples. The g-C_3N_4, 0TC-300, and XTC-300 composites are photoactive towards hydrogen generation both under visible light and simulated sunlight. The average rate of hydrogen production within 6 h is illustrated in Fig. 8a. Despite the conduction band potential of g-C_3N_4 being more negative than the reduction potential of H^+/H_2, the bare g-C_3N_4 is not very efficient at photocatalytically generating hydrogen. Photocatalytic hydrogen generation rate over 0TC-300 is more than three times greater than that over bare g-C_3N_4, illustrating the activity enhancement invoked by hydrothermal treatment in the H_2O_2-NH_4OH solvent. Li et.al[38] found that O-doped g-C_3N_4 would be formed by H_2O_2 hydrothermal procedure, and exhibits superior photoreactivity towards H_2 evolution under visible light irradiation. Thus, we deduced that improvement of H_2 evolution for 0TC-300 is from the introduction of oxygen atoms into g-C_3N_4. The average H_2 evolution rates of all the composites are higher than that of 0TC-300, which denotes that the impregnation of Ti species provides better quantum efficiency. When the loading amount of TiO_2 is gradually increased, the photocatalytic activity is firstly increased and then decreased. Under the irradiation of visible light, the optimum contents of TiO_2 are 15.3% and 26.2%, which H_2 evolution rate is about 4.6 times that of pristine g-C_3N_4. Higher content of TiO_2 nanoparticles would tend to aggregate together and may decrease the efficient utilization of g-C_3N_4 for visible light. However, in the case of simulated sunlight irradiation, the optimum content of TiO_2 is 26.2% and the hydrogen production rate is higher than that under visible light irradiation. This is due to the involvement of TiO_2 into the hydrogen production and the improvement of incident energy.

Fig. 7c and Fig. 8b show the influence of the calcination temperature on 20TC for the hydrogen production under visible irradiation. It is evident that the composite calcined at 300 °C exhibits the best photocatalytic activity. It is generally believed that higher crystallinity is beneficial to the transfer of electrons and holes. As shown in Fig. 2b, the 20TC composite calcined at 300 °C exhibits low crystalline then 400 °C, whereas, 20TC-300 has higher photocatalytic activity. Meanwhile, we have observed that the diffraction pattern of g-C_3N_4 ((002) peak) in the composite shifts to lower angle and returns to the original position of bulk g-C_3N_4 at the calcinations temperature of 400 °C (Fig.2b). Thus, we deduce that the decrease in activity may come from the destruction of the coordination between Ti species and g-C_3N_4 on 400 °C. When the temperature reaches 500 °C, the photocatalytic activity is almost completely wiped out because of the sublimation of g-C_3N_4.

Based on the above result, we further study the function of the coordination between Ti species and g-C_3N_4 in the composite during the processes of hydrogen production. Thus, we synthesized TiO_2/g-C_3N_4 composite (20TC-300W) via microwave-assisted route instead of hydrothermal reaction (all other processes are the same as 20TC-300). In order to eliminate the impact of g-C_3N_4, 0TC-300 was used in the synthesis of 20TC-300W and TC-300M (with TiO_2 content of 26wt%). The comparison of XRD pattern for 0TC-300, 20TC-300 and 20TC-300W are shown in Fig. 9.

Compared to bare g-C_3N_4, there is no obvious shift of the g-C_3N_4 (002) peak in 20TC-300W sample, indicating that there is no coordination between Ti species and g-C_3N_4 under the mild condition.

The photocatalytic hydrogen production results are presented in Fig. 7d and Fig. 8b. It can be seen that the physical mixing almost had no effect on the hydrogen evolution. The photocatalytic activity of 20TC-300W is higher than that of 0TC-300, which indicates the hybrid of g-C_3N_4 with TiO_2 can improve the photocatalytic activity. However, 20TC-300 displays better photocatalytic H_2 production performance than 20TC-300W. From the above result, it can be inferred that the coordination between Ti species and g-C_3N_4 in the composite plays a part for the hydrogen production.

In order to investigate the photocatalytic stability of 20TC-300 sample, the photocatalytic recycle experiment was carried out. As shown in Fig. 10, the H_2 production ability is stable

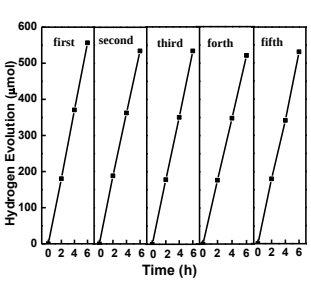

Fig.10. Stable hydrogen evolution over 20TC-300 sample under visible light irradiation. The reactor was flushed with Ar every six hours to evacuate the H_2 produced.

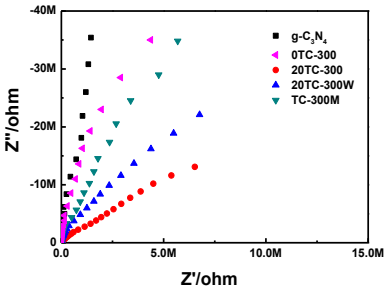

Fig. 11. EIS Nyquist plots of the photocatalysts

during the 30 h reaction, indicating its good stability.

3.3 Possible photocatalytic mechanism of the Ti species modified g-C_3N_4

It is reported that increasing of the electric conductivity can improve the charge-carrier density of g-C_3N_4, and also favoring the transport of charge-carrier.[22] Herein, electrochemical impedance measurements by means of two probe method were employed to investigate the conductivity of the samples. The tablet of the sample was clamped on a copper sample holder assembly between two copper leads. In electrochemical spectra, the high frequency arc corresponds to the charge transfer limiting process and can be attributed to the double-layer capacitance in parallel with the charge transfer resistance in the sample tablet. As seen from Fig. 11, the arc radius from the electrochemical impedance spectroscopy (EIS) Nyquist plots of 0TC-300 is slightly smaller than bare g-C_3N_4, suggesting that the process of hydro-thermal treatment in the H_2O_2-NH_4OH solvent can improve the conductivity of g-C_3N_4 inconspicuously. Besides, the introduction of TiO_2 can also enhance the electric conductivity. By comparison, 20TC-300 possesses the highest electric conductivity. Thus, it is speculated that the highly electric conductivity of 20TC-300 not only comes from the introduction of TiO_2, but also from the coordination between Ti species with the lone-pair electrons on N atom in g-C_3N_4. In a word, the micro structural change of g-C_3N_4 via coordination with Ti species during the hydrothermal treatment improves the electric conductivity of g-C_3N_4 and makes charge transfer easier.[39]

To further investigate the charge carriers transfer behavior, the photoluminescence measurement was employed (Fig. 12a). It is interesting that the main emission wavelength of bare g-C_3N_4 at 460 nm is shifted to 450 nm after the hydrothermal treatment. The PL signal is often considered as the radioactive recombination of photo-induced electrons and holes. The shift of emission wavelength for 0TC-300 may be due to the changes of surface states during the hydrothermal treatment in the H_2O_2-NH_4OH solvent. After the introduction of Ti species, the main wavelength of the composites is still at 450 nm and the intensity is lower than that of 0TC-300. The lower PL emission intensity indicates lower recombination efficiency of the electron/hole pair.[40] Among the three hybrid samples, 20TC-300 shows the lowest PL intensity, indicating more excitons of 20TC-300 transfer via other way instead of radiative paths.[41] This result implies that both constituted of heterojunction with TiO_2 and coordination with Ti species can

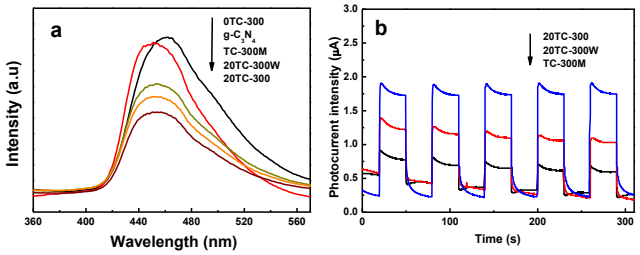

Fig. 12. (a) Photoluminescence (PL) spectra of the photocatalysts, (b) Photocurrent responses of the photocatalyst under visible light irradiation.

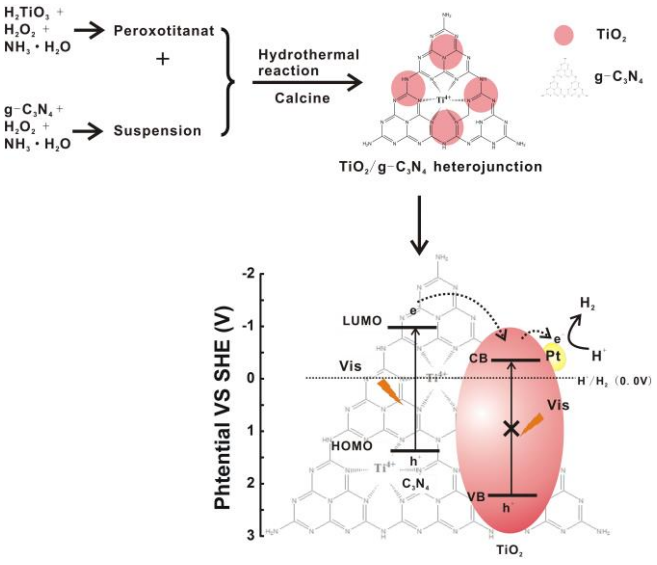

Scheme 1. The formation and photocatalytic mechanism scheme of the Ti species modified g-C_3N_4.

obviously favor the separation and transition of photogenerated carriers in g-C_3N_4 and enhance the photocatalytic activity.

Photocurrents were also measured for the three hybrid samples to further investigate the transmission of photo-generated carriers. As shown in Fig. 12b, 20TC-300 has the strongest photocurrent under visible light irradiation. The photocurrent of 20TC-300 is about two times as high as that of the 20TC-300W.

On the basis of the photocatalytic H_2 generation and test results, the proposed process and mechanism for the Ti species modification and the promotion photocatalytic H_2 generation performance is proposed in Scheme 1. Firstly, metatitanic acid reacted with the mixture of ammonium hydroxide and hydrogen peroxide, and then converted to peroxotitanate solution.[31] Meanwhile, bare g-C_3N_4 was dispersed into the mixture solution of ammonium hydroxide and hydrogen peroxide and treated by an ultrasonic method. Secondly, when the peroxotitanate solution and suspension of g-C_3N_4 were mixed together, peroxotitanate was adsorbed on the surface of the g-C_3N_4. Under hydrothermal conditions, peroxotitanate could be converted into TiO_2 nanoparticles, and in the meanwhile Ti species could drop into the bulk phase of g-C_3N_4 by coordination. Thirdly, due to the coordination between Ti species with g-C_3N_4, the photo-induced electrons in g-C_3N_4 are becoming easier to transfer to the heterointerface

of the composite. Then, because the lowest unoccupied molecular orbital (LUMO) level of g-C_3N_4 (-1.20 eV)[42] is more negative than the conduction band (CB) edge of TiO_2 (-0.50 eV),[19] the excited electrons on LUMO of g-C_3N_4 can inject into the CB of TiO_2. Finally, H^+ is reduced to hydrogen molecule after accepting the electrons on the Pt particles or CB of TiO_2.

Conclusions

A Ti species modified g-C_3N_4 photocatalyst was synthesized via an in-situ hydrothermal route and calcinations. This synthetic method not only results in the fabrication of TiO_2/g-C_3N_4 heterojunctions, but also leads to a microstructure modification of g-C_3N_4 by Ti species. The coordination between Ti species and g-C_3N_4 improves the electric conductivity of composite and makes charge transfer easier. Meanwhile, the heterojunction between TiO_2 and g-C_3N_4 can also improve the separation efficiency of photo-generated carriers in the process of photocatalysis. Under visible-light irradiation, the optimum contents of TiO_2 are 15.3% and 26.2%, and the photocatalytic activity of the obtained heterojunctions is about 4.6 times that of pristine g-C_3N_4 for H_2 evolution. This work could provide deeper insight into the enhanced mechanisms of π-conjugated molecules hybridized semiconductors.

Acknowledgements

This work was supported by the National Natural Science Foundation of China (No. 21406054,21376061), Natural Science Foundation of Hebei Province (B2015208005), the Program for New Century Excellent Talents in University (No. NCET-12-0686), Natural Science Foundation for Distinguished Young Scholar of Hebei Province (B2015208010), and Scientific Research Foundation for High-Level Talent in University of Hebei Province (GCC2014057), and the Foundation of Hebei University of Science and Technology (No. 2014PT90).

Notes and references

1 S. Obregón and G. Colón, *Appl. Catal. B*, 2014, **144**, 775.
2 D. Li, X. W. Cheng, X. J. Yu and Z. P. Xing, *Chem. Eng. J*. 2015, **279**, 994.
3 X. C. Wang, K. Maeda, A. Thomas, K. Takanabe, G. Xin, J. M. Carlsson, K. Domen and M. Antonietti, *Nat. Mater*., 2009, **8**, 76.
4 L. Shi, L. Liang, F. X. Wang, M. S. Liu, T. Liang, K. L. Chen and J. M. Sun, *RSC Adv*., 2015, **5**, 63264.
5 Z. Y. Zhang, J. D. Huang, Q. Yuan and B. Dong, *Nanoscale*, 2014, **6**, 9250.
6 H. L. Gao, S. C. Yan, J. J. Wang, Y. A. Huang, P. Wang, Z. S. Li and Z. G. Zou, *Phys. Chem. Chem. Phys*.,2013, **15**, 18077.
7 T. Sano, S. Tsutsui, K. Koike, T. Hirakawa, Y. Teramoto, N. Negishi and K. Takeuchi, *J. Mater. Chem. A*, 2013, **1**, 6489.
8 X. S. Zhang, J. Y. Hu and H. Jiang, *Chem. Eng. J*., 2014, **256**, 230.
9 S. X. Min and G. X. Lu, *J. Phys. Chem. C*, 2012, **116**, 19644.
10 G. H. Dong, K. Zhao and L. Z. Zhang, *Chem. Commun*., 2012, **48**, 6178.
11 S. Z. Hu, F. Y. Li, Z. P. Fan, F. Wang, Y. F. Zhao and Z. B. Lv, *Dalton Trans.,* 2015, **44**, 1084.
12 S. C. Yan, Z. S. Li and Z. G. Zou, *Langmuir*, 2010, **26**, 3894.
13 G. Liu, P. Niu, C. H. Sun, S. C. Smith, Z. G. Chen, G. Q. Lu and H. M. Cheng, *J. Am. Chem. Soc*., 2010, **132**, 11642.
14 J. Liu, Y. Liu, N. Y. Liu, Y. Z. Han, X. Zhang, H. Huang, Y. Lifshitz, S. T. Lee, J. Zhong and Z. H Kang, *Science*, 2015, **347**, 970.
15 X. J. Wang, Q. Wang, F. T. Li, , W. Y. Yang, Y. Zhao, Y. J. Hao and S. J. Liu, *Chem. Eng. J*., 2013, **234**, 361.
16 R. C. Pawar, V. Khare and C. S. Lee, *Dalton Trans.,* 2014, **43**, 12514.
17 F. T. Li, S. J. Liu, Y. B. Xue, X. J. Wang, Y. J. Hao, J. Zhao, R. H. Liu and D. S. Zhao, *Chem. Eur. J*., 2015, **21**,10149.
18 F. T. Li, Y. Zhao, Q. Wang, X. J. Wang, Y. J. Hao, R. H. Liu and D. S. Zhao, *J. Hazard. Mater*., 2015, **283**, 371.
19 L. A Gu, J. Y. Wang, Z. J. Zou and X. J. Han, *J. Hazard. Mater*., 2014, **268**, 216.
20 K. Sridharan, E. Jang and T. J. Park, *Appl. Catal. B*, 2013, **142–143**, 718.
21 G. G. Zhang, M. W. Zhang, X. X. Ye, X. Q. Qiu, S. Lin and X. C. Wang, *Adv. Mater*., 2014, **26**, 805.
22 Y. J. Zhang, T. Mori, J. H. Ye and M. Antonietti, *J. Am. Chem. Soc*., 2010, **132**, 6294.
23 S. Zhou, Y. Liu, J. M. Li, Y. J. Wang, G. Y. Jiang, Z. Zhao, D. X. Wang, A. J. Duan, J. Liu and Y. C. Wei, *Appl. Catal. B*, 2014, **158–159**, 20.
24 W. Li, C. Li, B. Chen, X. L. Jiao and D. R. Chen, *RSC Adv*., 2015, **5**, 34281.
25 Y. Guo, F. Kong, S. Chu, L. L. Luo, J. C. Yang, Y. Wang and Z. G. Zou, *RSC Adv*., 2012, **2**, 5585.
26 X. X. Zou, G. D. Li, Y. N. Wang, J. Zhao, C. Yan, M. Y. Guo, L. Li and J. S. Chen, *Chem. Commun*., 2011, **47**, 1066.
27 J. G. Yu, S. H. Wang, J. X. Low and W. Xiao, *Phys. Chem. Chem. Phys*., 2013, **15**, 16883.
28 Z. A. Huang, Q. Sun, K. L. Lv, Z. H. Zhang, M. Li and B. Li, *Appl. Catal. B*, 2015, **164**, 420.
29 X. S. Zhou, F. Peng, H. J. Wang, H. Yu and Y. P. Fang, *Chem. Commun*., 2011, **47**, 10323.
30 S. S. Ma, J. J. Xue, Y. M. Zhou, Z. W. Zhang, Z. L. Cai, D. B. Zhu and S. Liang, *RSC Adv*., 2015, **5**, 64976.
31 X. J. Wang, W. Y. Yang, F. T. Li, Y. B. Xue, R. H. Liu and Y. J. Hao, *Ind. Eng. Chem. Res*., 2013, **52**, 17140.
32 R. Murugan, V. Thangadurai and W. Weppner, *Angew. Chem. Int. Ed*., 2007, **46**, 7778.
33 S. Tonda, S. Kumar, S. Kandula and V. Shanker, *J. Mater. Chem. A*, 2014, **2**, 6772.
34 J. Tauc, *Mater. Res. Bull*.,1970, **5**, 721.
35 Y. D. Hou, X. C. Wang, L. Wu, X. F. Chen, Z. X. Ding, X. X. Wang and X. Z. Fu, *Chemosphere*, 2008, **72**, 414.
36 K. Dai, L. H. Lu, C. H. Liang, Q. Liu and G. P. Zhu, *Appl. Catal. B*, 2014, **156–157**, 331.
37 L. Q. Ye, J. Y. Liu, Z. Jiang, T. Y. Peng and L. Zan, *Appl. Catal. B*, 2013, *142–143*, 1.
38 J. H. Li, B. Shen, Z. H. Hong, B. Z. Lin, B. G. Gao and Y. L. Chen, *Chem Commun*, 2012, **48**, 12017.
39 M. Zhang, X. J. Bai, D. Liu, J. Wang and Y. F. Zhu, *Appl. Catal. B*, 2015, **164**, 77.
40 L. L. Chen, W. X. Zhang, C. Feng, Z. H. Yang and Y. M. Yang, *Ind. Eng. Chem. Res*., 2012, **51**, 4208.
41 M. Shalom, S. Inal, C. Fettkenhauer, D. Neher and M. Antonietti, *J. Am. Chem. Soc*., 2013, **135**, 7118.
42 T. T. Li, L. H. Zhao, Y. M. He, J. Cai, M. F. Luo and J. J. Lin, *Appl. Catal. B*, 2013, **129**, 255.